A&A, 689, L10 (2024)
https://doi.org/10.1051/0004-6361/202451856

Astronomy & Astrophysics

LETTER TO THE EDITOR

Bright unintended electromagnetic radiation from second-generation Starlink satellites

C. G. Bassa[1,⋆,⋆⋆], F. Di Vruno[2,3,⋆⋆], B. Winkel[4,3,⋆⋆], G. I. G. Józsa[4,5,3,⋆⋆], M. A. Brentjens[1], and X. Zhang[6]

[1] ASTRON, Netherlands Institute for Radio Astronomy, Oude Hoogeveensedijk 4, 7991 PD Dwingeloo, The Netherlands
[2] Square Kilometre Array Observatory, Lower Withington, Macclesfield, Cheshire SK11 9FT, United Kingdom
[3] European Science Foundation, Committee on Radio Astronomy Frequencies, 1, quai Lezay Marnésia BP 90015, F-67080 Strasbourg Cedex, France
[4] Max-Planck-Institut für Radioastronomie, Auf dem Hügel 69, 53121 Bonn, Germany
[5] Department of Physics and Electronics, Rhodes University, PO Box 94, Makhanda 6140, South Africa
[6] LESIA, Observatoire de Paris, Université PSL, CNRS, 5 place Jules Janssen, 92195 Meudon, France

Received 9 August 2024 / Accepted 29 August 2024

ABSTRACT

We report on the detection of unintended electromagnetic radiation (UEMR) from the second-generation of Starlink satellites. Observations with the LOFAR radio telescope between 10 to 88 MHz and 110 to 188 MHz show broadband emission covering the frequency ranges from 40 to 70 MHz and 110 to 188 MHz from the v2-Mini and v2-Mini Direct-to-Cell Starlink satellites. The spectral power flux density of this broadband UEMR varies from satellite to satellite, with values ranging from 15 to 1300 Jy, between 56 and 66 MHz, and from 2 to 100 Jy over two distinct 8 MHz frequency ranges centered at 120 and 161 MHz. We compared the detected power flux densities of this UEMR to that emitted by the first generation v1.0 and v1.5 Starlink satellites. When correcting for the observed satellite distances, we find that the second-generation satellites emit UEMR that is up to a factor of 32 stronger compared to the first generation. The calculated electric field strengths of the detected UEMR exceed typical electromagnetic compatibility standards used for commercial electronic devices as well as recommended emission thresholds from the Radiocommunication Sector of the International Telecommunications Union (ITU-R) aimed at protecting the 150.05–153 MHz frequency range allocated to radio astronomy. We characterize the properties of the detected UEMR with the aim of assisting the satellite operator with the identification of the cause of the UEMR.

Key words. light pollution – space vehicles – telescopes – surveys

1. Introduction

With the miniaturization of satellites and the rapid commercialization of spaceflight, the number of satellites in orbit around the Earth has dramatically increased since around 2016 (see McDowell 2020). Since then, several commercial companies have started to mass produce and launch large numbers of satellites to offer various communication services, primarily broadband internet and mobile connectivity. Satellites in such constellations are typically launched into shells of specific orbital altitude and orbital inclination to optimize coverage for specific geographic latitudes.

This growth in the number of satellites has worrisome implications for astronomy (Walker et al. 2020a,b, 2021) as the probability that satellites are passing through the fields of view of ground-based telescopes (as well as space-based) is drastically increasing, and sunlight reflected from these satellites, as well as radio signals emitted by them, are detectable by astronomical instruments (e.g., Tyson et al. 2020; Michałowski et al. 2021; Mróz et al. 2022; Kruk et al. 2023). Assessing the impact of these satellite constellations on different astronomical observatories and science cases is an increasingly important topic of recent research (e.g., Green et al. 2022; Bassa et al. 2022; Barentine et al. 2023; Lang et al. 2023; Kovalev et al. 2023; Hainaut & Moehler 2024).

For radio astronomy, the use of the radio spectrum is regulated by the Radiocommunication Sector of the International Telecommunication Union (ITU-R), which publishes the relevant international treaty in the form of the Radio Regulations. These regulations cover the intentional use of the radio spectrum for different applications (or services) such as communication, remote sensing, navigation, as well as astronomy. It considers wanted and unwanted emission, for example that due to out-of-band emission from spectral side-lobes. In particular, the ITU-R allocates several frequency ranges to the radio astronomy service. Rec. ITU-R RA.769-2 provides thresholds on the received power (or power flux densities) that must not be exceeded by other active radio services in these bands. As these bands focus on spectral lines affected by Galactic Doppler shifts, the frequency ranges are relatively narrow.

In Di Vruno et al. (2023) we introduced the concept of unintended electromagnetic radiation (UEMR), referring to any electromagnetic radiation that is radiated by (or leaking from)

⋆ Corresponding author; bassa@astron.nl
⋆⋆ Member of the IAU Centre for the Protection of the Dark and Quiet Sky from Satellite Constellation Interference (IAU CPS).

electrical devices and systems on board satellites, and not necessarily related to the generation and transmission of wanted electromagnetic radiation from antennas used for communication, for example. Through simulations of the aggregate effect of UEMR emitted by satellites in various large satellite constellations, we found that the radiation levels required to comply with ITU-R specified interference thresholds for frequency ranges assigned to radio astronomy, would be quite constraining when compared to typical electromagnetic compatibility standards used for commercial devices on Earth. Unfortunately, the detected levels of both narrowband and broadband UEMR at frequencies between 110 and 188 MHz of dozens of satellites belonging to the SpaceX Starlink constellation showed emissions above these calculated thresholds (Di Vruno et al. 2023). This detection of UEMR from the Starlink constellation has since been independently confirmed by Grigg et al. (2023).

In Di Vruno et al. (2023) we argued that while narrowband UEMR detected at 143.050 MHz could be attributed to reflections from the French GRAVES Space Surveillance Radar, other narrow- and broadband emissions were intrinsically radiated by the satellites. Doppler analysis of the narrowband emissions provides further evidence (Bassa et al., in prep.) of this intrinsic origin. Triggered by the initial detections of satellite UEMR we have initiated an observing program to investigate and characterize UEMR from satellites within different satellite constellations (e.g., OneWeb, IRIDIUM Next, Swarm, Planet Labs, BlueWalker), and different hardware versions of satellites within a constellation (Starlink). As part of these observations, and those triggered by a request (C. Lonsdale, priv. comm.) to confirm circumstantial evidence for possible UEMR detected in the EDGES epoch-of-reionization experiment (Bowman et al. 2008), we report on the detection of bright and broadband UEMR from satellites of the second generation of Starlink.

2. Observations and analysis

2.1. Observations

The observations reported here closely follow the observational setup used and detailed in Di Vruno et al. (2023), where satellites are detected by letting them pass through the telescope beam pattern. Two one-hour observations were obtained using the central six stations of the LOFAR radio telescope (van Haarlem et al. 2013) in the Netherlands on July 19, 2024, one covering frequencies from 10 to 88 MHz using the low-band antennas (LBAs) in the LBA_OUTER configuration, the other 110 to 188 MHz with the high-band antennas (HBAs). Signals from these stations were coherently added in the `COBALT` beamformer (Broekema et al. 2018) to form 91 tied-array beams (TABs), tiling out the primary station beam in hexagonal rings with separations near the TAB full width at half maximum (FWHM) of 42′ for the LBA observation, and 24′ for the HBA observation. For each tied-array beam, dynamic spectra with total intensity (Stokes I) were recorded at 41.94 ms time resolution and 12.2 kHz frequency resolution. To minimize the distance between the telescope and satellites passing through the beam pattern, the TABs for both observations tracked equatorial positions, which culminated near zenith (maximum elevation 87°.5) half-way through the one-hour integration.

2.2. Analysis

The dynamic spectra were analyzed and searched for the presence of satellite UEMR using an adapted version of the method outlined in Di Vruno et al. (2023). First, we retrieved orbital elements in the form of two-line element sets (TLEs), from publicly available catalogs. These orbital elements are derived from observations by the United States Space Force (USSF)[1]. This approach allows searching for the UEMR of any satellite in the USSF catalog, whereas in Di Vruno et al. (2023) we used ephemerides provided by SpaceX that are only available for Starlink satellites. Using these orbital elements, we used the `Skyfield` software to compute the predicted trajectory of each satellite through the beam pattern of both observations and determine ingress, midpoint, and egress times for the station beam and for each TAB that the satellite passes through.

Next, for each satellite passing through the beam pattern, we extracted a time range, centered on the predicted midpoint of the passage, from the dynamic spectra of each of the 91 TABs. The width of this time range was chosen depending on the angular velocity of the satellite on the sky and the FWHM of the station beam, and varied from 12 to 40 s. Similarly, to increase the signal-to-noise ratio, the extracted dynamic spectra are averaged to a lower time resolution by a factor $n_{\rm bin}$ from the native 41.94 ms time resolution. We ensured that the duration of the passage through a TAB is covered by at least four averaged time samples.

The extracted dynamic spectra of each TAB were bandpass-calibrated by normalizing with the median of the dynamic spectra of the TABs where the satellite did not pass through. This approach has the advantage that the effect of low-level terrestrial radio frequency interference (RFI), which appears similar in power in all beams, is minimized. After this normalization step, small variations in intensity (∼1%) between the different tied-array beams remain, due to differences in sky temperatures and astrophysical sources. We removed these by defining the on-source spectrum as the time range during which the satellite is predicted to be located inside the primary station beam, and the off-source spectrum as the time range it is outside of this area, and further normalizing the spectra by the median intensity of each channel for the off-source time range.

We used the off-source time range to determine the frequency dependent rms of the noise, and used this as input for the radiometer equation to flux-calibrate the normalized dynamic spectra. The radiometer equation relates the rms noise to the spectral flux density of each time and frequency bin in the dynamic spectra through the system temperature and the telescope gain, as well as the time ($t_{\rm samp}$ = 41.94 $n_{\rm bin}$ ms) and frequency resolution ($\Delta\nu$ = 12.2 kHz) and the number of polarizations recorded ($n_{\rm pol}$ = 2). To determine the frequency dependent system temperature and telescope gain for the LOFAR LBA and HBA observation, we used the method by Kondratiev et al. (2016), which models the effective area, the station beam model, antenna and sky temperature, together with the beamformer coherency based on the number of stations used to form the tied-array beams, as well as the sky pointing of the beams. This approach is the same as in Di Vruno et al. (2023), except for the frequency-dependent calibration, which is strictly necessary for the LBA data.

For each satellite, we used the predicted mid-point times of each beam through which it passed to align the flux-density calibrated dynamic spectra in time, and computed the beam-averaged dynamic spectrum to increase the signal-to-noise ratio and be more sensitive to faint UEMR. Since the satellites do not necessarily pass through the center of each tied-array beam, the average of the flux-density calibrated spectra will underestimate

[1] Distributed through `www.space-track.org`

the actual flux density of the satellite compared to a satellite that actually passed through the center of each TAB. Hence, we used the angular response of a TAB (using the FWHM and approximated with a Gaussian) to compute the weighting of all beams and used this to correct the flux density scale. This correction is frequency dependent since the TAB FWHM scales with observing frequency.

The resulting aligned and averaged dynamic spectra were inspected for the presence of both narrowband and broadband emission whose temporal width is consistent with the expected passage duration through the TAB FWHM. In cases where this emission is detected, the temporal profile is fitted with a Gaussian to represent the beam shape, and to provide power flux density measurements and time offsets due to the satellite running ahead or behind predictions. For narrowband emission, we subtracted the spectral baseline of the surrounding 0.5 MHz to provide measurements relative to broadband emission. To allow comparison with our earlier measurements from Di Vruno et al. (2023), we used the same narrowband frequencies (125, 135, 143.05, 150, and 175 MHz) and broadband frequency ranges (116–124, 150.05–153, and 157–165 MHz) for the HBA observation[2]. For the LBA observation, we chose narrowband frequencies at 25, 50, and 75 MHz to check for the presence of the harmonics spaced at 25 MHz intervals that were reported earlier by Di Vruno et al. (2023). Broadband frequency ranges correspond to the 37.5–38.25 MHz and 73–74.6 MHz frequency ranges where radio astronomy has a secondary and primary ITU-R allocation (see Rec. ITU-R RA.769-2 and Radio Regulations, Vol. 1, footnote 5.149), respectively. We also include the 50–54 MHz frequency range, which is assigned for radio amateur usage, and 56–61 MHz and 61–66 MHz, where the strongest signals are detected.

The figures in Appendix A show examples of aligned and averaged dynamic spectra for several satellites in the different observing bands, while the tables in Appendix B provide lists of the detected Starlink satellites, the properties of the passage through the LOFAR beam pattern, and the power flux density measurements.

3. Results

A total of 141 Starlink satellites were predicted to pass through at least one tied-array beam in the LBA observation covering 10–88 MHz, while 97 satellites did so for the HBA observation spanning 110–188 MHz. Publicly available information from Jonathan McDowell[3] and Gunther Krebs[4] indicates that the observed satellites are of four different versions currently in orbit. Satellite versions v1.0 and v1.5 are from the first generation of Starlink satellites, which were also observed in the 2022 observation presented in Di Vruno et al. (2023). The other two satellite versions are from the second generation of Starlink: the normal v2-Mini satellite and the direct-to-cell (DTC) version, which offers cellular mobile phone coverage. Orbital launches of the v2-Mini satellite versions started in February 2023, initially into 43° inclined orbits, and since August 2023 into orbits with 53° inclination. Launches with the DTC type v2-Mini's started in January 2024 and are occasionally launched together with the normal v2-Mini satellites. The DTC version of the v2-Mini satellites are currently all in 53° inclined orbits.

In the HBA observation, all 97 Starlink satellites are detected, either through narrowband emission, predominantly at 125 MHz, or broadband emission over parts of or most of the 110–188 MHz frequency range. The detected signals from the v1.0 and v1.5 satellite versions are consistent in flux density and spectral properties to those of the satellites we detected in the analysis of the 2022 observation in this frequency range (Di Vruno et al. 2023). The aligned and averaged dynamic spectra of the second-generation v2-Mini satellite versions appear distinctly different, as these do not show the narrowband emission at 125, 135, and 150 MHz, but instead show significantly brighter broadband UEMR than the v1.0 and v1.5 versions.

At the LBA frequencies between 10 and 88 MHz, UEMR from the v2-Mini and v2-Mini DTC versions is clearly detected for 27 of the 29 observed satellites; it is exceedingly bright, reaching power flux densities of hundreds of janskys, and in a few cases even exceeding 1 kJy. The emission is predominantly constrained to a ∼10 MHz band centered around 61 MHz, but in some cases the broadband emission is detectable down to frequencies of around 40 MHz. The broadband UEMR varies in brightness from satellite to satellite, and tends to peak at different frequencies between 60 and 64 MHz. The v1.0 and v1.5 version satellites are not detected in the LBA data, neither through broadband emission nor at the narrowband frequencies at 25, 50, and 75 MHz. In the few cases where signals were present in the aligned and averaged spectra, they could be explained by the strong UEMR from v2-Mini or v2-Mini DTC satellites that were also in or near the station beam at that time as a result of the increasing density of satellites in the sky. As the v1.0 and v1.5 satellite versions emit narrowband UEMR at 125, 150, and 175 MHz, we suggested in Di Vruno et al. (2023) that these may be harmonics of a 25 MHz clock signal on board the satellite, and that we would expect emission at the fundamental frequency of 25 MHz and the harmonics at 50 and 75 MHz. While the 25 MHz frequency is lost due to terrestrial RFI, the LBA observations show that if present, the narrow- or broadband UEMR at 50 and 75 MHz must have power flux densities below $S_\nu < 10$ Jy (3σ).

Figure 1 provides an overview of the power flux density measurements at the different narrowband frequencies and broadband frequency ranges, their distances to the telescope at the time of detection, and the satellite versions. It is clear that the power flux densities of the v2-Mini and v2-Mini DTC Starlink satellites are higher than those of the first generation. However, the v2-Mini and v2-Mini DTC versions were observed at smaller distances as these satellites operate at lower orbital altitudes. To determine whether the UEMR emitted by the second generation of Starlink satellites is intrinsically brighter, we corrected the observed power flux densities by scaling them to a fixed distance of 1000 km, as shown in Fig. 2. This approach also has the advantage that these normalized power flux densities can be directly related to the electric field strength emitted by the satellites, if received by a detector at a distance of 10 m and integrating over a 120 kHz bandwidth. This implicitly assumes that the emitted UEMR is isotropic, which likely is not the case, but allows further comparison to commercial electromagnetic compatibility (EMC) standards that we used in Di Vruno et al. (2023). From Fig. 2 we find that intrinsic levels of broadband UEMR emitted by the observed satellites from the second generation of Starlink (the v2-Mini and v2-Mini DTC versions) are higher than those observed from the first-generation satellites.

In the LBA band, UEMR from the observed v2-Mini and v2-Mini DTC satellites shows spectral structure over the entire

[2] The 175 MHz frequency has become unavailable due to the use of this frequency by digital audio broadcasting.
[3] https://planet4589.org/space/con/star/stats.html
[4] https://space.skyrocket.de/doc_sdat/starlink-v1-0.htm and associated links.

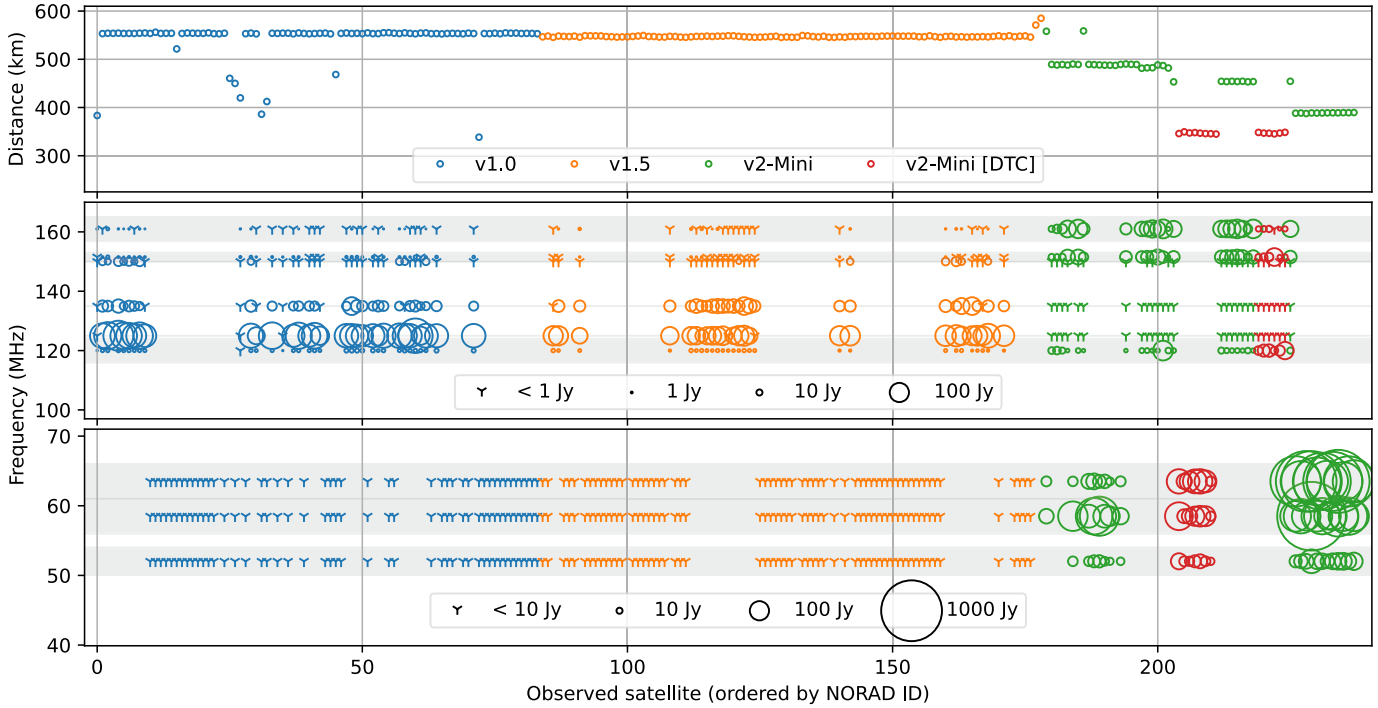

Fig. 1. Distances and power flux density measurements of Starlink satellites that passed through the beam pattern of the two 1 h LOFAR observations. The horizontal axis denotes the number of satellites that were observed, ordered by their NORAD catalog identifier. As this identifier sequentially increases with each launched satellite, this axis is essentially ordered in time. All satellites were observed near zenith, and hence their distances are comparable to their orbital altitudes. Power flux density measurements at the different narrowband frequencies or broadband frequency ranges are indicated with circles, where the size of the circle corresponds to the measured flux density. Nondetections are denoted by the ϒ symbol. The horizontal gray lines and bands indicate the frequency ranges that were used for the flux density determination. There are separate legends for the LBA band from 10–88 MHz and the HBA band from 110–188 MHz. The different Starlink satellite versions are indicated with different colors.

frequency range where UEMR is detected. This structure consists of a "comb" of regularly spaced peaks in frequency. Power spectra of this emission at the 12.2 kHz frequency resolution between 56 and 66 MHz show significant peaks at multiple, harmonically related, peaks at frequencies of 27.5, 36.66, 55, 110, and 220 kHz for the v2-Mini satellites, and at 37.5, 50, 75, and 150 kHz for the v2-Mini DTC satellites. This shows that this spacing is distinctly different between the v2-Mini and v2-Mini DTC satellite versions that were observed. Due to variations in the power of the spectral harmonics, we cannot identify a fundamental frequency of these combs. Spectral structure is less apparent for the UEMR detections in the HBA band. Power spectra over the two frequency ranges between 116–124 and 157–165 MHz show that some of the version v1.5 satellites observed have a comb with a fundamental frequency at 50 kHz in the 157–165 MHz band, similar to what was seen in our earlier observations of satellites of this version (Di Vruno et al. 2023). The v2-Mini satellites observed predominantly show periodic signals at frequencies of 48.8, 65, and 97.5 kHz in the 157 to 165 MHz band, while most of the v2-Mini DTC satellites show a comb with 50 or 150 kHz spacing in the lower band from 116 to 124 MHz. For these combs, no fundamental frequency can be identified due to the satellite-to-satellite power variations of the harmonics.

4. Discussion and conclusions

We find that the second generation of Starlink satellites that we observed with LOFAR emit higher levels of unintended electromagnetic radiation (UEMR) over a broader frequency range compared to that emitted by the first generation of Starlink satellites. Our observations show that in the 150.05–153 MHz primary radio astronomy band, the broadband UEMR of the second-generation v2-Mini and v2-Mini DTC satellites is, on average, 15 dB and 7 dB brighter than that of the first-generation v1.0 and v1.5 Starlink satellites. On a linear scale, this corresponds to factors of 32 and 5, respectively. As is evident from Fig. 2, this trend is also present in the 116–124 MHz and 157–165 MHz bands, and in the frequency bands from 50 to 66 MHz where the satellites from the first generation are not detected. On the other hand, the strong narrowband UEMR that is seen in the v1.0 and v1.5 satellites at 125, 135, and 150 MHz appears to be absent in the v2-Mini and v2-Mini DTC satellites. While this is an improvement, it is completely negated by the stronger broadband UEMR, which affects a significantly larger part of the observed frequency range.

The issue of the higher levels of UEMR from the second-generation Starlink satellites is further exacerbated by the lower orbits in which these satellites operate. These satellites are used in the (modified) Generation 2 Starlink constellation, for which the US Federal Communications Commission (FCC) has approved operational orbits at 448 and 482 km for the v2-Mini satellites, and 360 km for the v2-Mini DTC satellites. As a result of these lower orbits and resulting smaller distances to Earth-based telescopes, the signals will be 30–130% brighter compared to the Generation 1 Starlink constellation, which mostly operates at orbital altitudes of 550 km.

In Di Vruno et al. (2023), we used the ITU-R recommended equivalent power flux density (EPFD) method (Rec. ITU-R M.1583-1; Rec. ITU-R S.1586-1) to simulate the aggregate impact of large numbers of satellites in several satellite con-

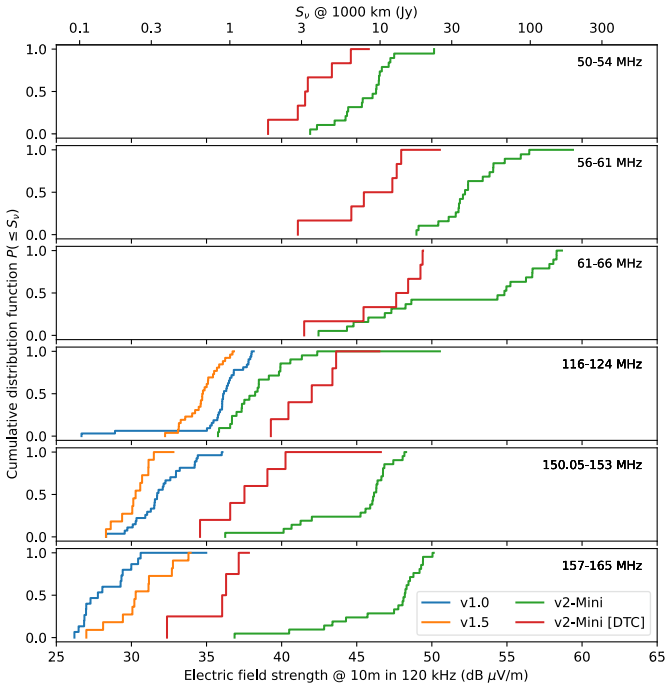

Fig. 2. Comparison of the intrinsic UEMR power flux densities for different broadband frequency ranges per Starlink satellite version. Each panel shows a cumulative distribution function of the power flux density measurements scaled to a distance of 1000 km (top axis) or represented as the electric field strength measured by a detector at 10 m distance using 120 kHz of bandwidth (bottom axis).

stellations and estimate their compatibility with ITU-R recommended interference thresholds. For the Generation 1 Starlink constellation of 4408 satellites in orbits at 550 km altitude, we found that the intrinsic electric field strength of an individual satellite had to remain below 11.7 dB [μV m^{-1}] to satisfy the −194 dB [W m^{-2}] ITU-R threshold for the radio astronomy band of 150.05–153 MHz (Rec. ITU-R RA.769-2). The intrinsic broadband UEMR from observed Starlink v1.0 and v1.5 satellites from the 2022 observation had electric field strengths of 21–39 dB [μV m^{-1}], already significantly exceeding that limit. These values also exceed typical commercial EMC standards (e.g., 30 dB [μV m^{-1}] from CISPR, see discussion in Di Vruno et al. 2023). Given that the Generation 2 Starlink constellation will consist of even more satellites than the Generation 1 constellation, that these satellites will be operating at lower orbital altitudes, and that this constellation will consist of the v2-Mini and v2-Mini DTC satellites that are now found to emit even stronger UEMR, we can conclude that the Rec. ITU-R RA.769-2 recommended interference threshold levels are exceeded even further in this radio astronomy band. The LOFAR observations presented here do not detect UEMR in the 73–74.6 MHz band allocated to radio astronomy. However, preliminary analysis of imaging observations of second-generation Starlink satellites with the NenuFAR telescope in France (Zarka et al. 2012), indicates that some may be detectable in that band (Zhang et al., in prep.). While they are beyond the scope of this paper, EPFD simulations of the Generation 2 Starlink constellation would be required to estimate the intrinsic electric field strengths required to keep the aggregate emission of UEMR of this constellation in accordance with the ITU-R recommendations.

Current wording of the ITU-R radio regulations (Radio Regulations) and recommendations (e.g., Rec. ITU-R RA.769-2, and related recommendations) discuss emissions in terms of wanted and unwanted emission related to signal transmission, where the unwanted emission is a byproduct of the wanted emission, for example due to out-of-band emission in the spectral domain. The UEMR as defined in our earlier paper (Di Vruno et al. 2023) appears to fall outside of these regulations. As such, UEMR is not subject to the ITU-R interference limits which protect certain parts of the spectrum for radio astronomical applications. Hence, we reiterate our earlier recommendation that UEMR from satellites should be considered in the regulatory processes.

The impact of the observed UEMR on radio astronomy likely varies between different science cases. The first-order effect will be a loss of sensitivity of low-frequency radio telescopes since the time and frequency ranges within an observation that are affected by satellite UEMR may have to be preemptively masked. However, given that low-frequency radio telescopes are primarily built for their large fields of view, the large numbers of satellites from current and future satellite constellations may lead to the situation that one or more satellites are present in the telescope's field of view at any given time. In this case, temporal masking of data will no longer provide useful data. This is the primary reason why broadband UEMR is particularly worrisome for radio astronomy; it increases the risk that the entire observing bandwidth is affected by UEMR for the entire duration of the observation. A second-order effect, primarily affecting interferometric telescope arrays, is that for closely spaced array elements (parabolic dishes or antenna stations), satellites will appear at the same sky location. As a result, UEMR will not decorrelate on the shortest baselines between individual array elements and may introduce artifacts on large spatial scales.

In contrast with this situation, astronomical radio observatories put a great deal of effort in mitigating their internally generated UEMR in all frequencies covered by their telescopes, as electrical devices needed to run telescopes are also prone to producing radio noise. Observatories such as LOFAR and the SKA Observatory go to great lengths, imposing extremely tight radio emission requirements on each of the subsystems that comprise the telescopes. In the SKA-Low case in Western Australia, some examples of this are the Central Processing Facility building, which is designed to shield all the computing equipment that performs the first processing of SKA-Low data, and the power and signal distribution boxes located in close proximity to SKA-Low antennas, having requirements that are more than 100 dB (10^{10} times) stricter than commercial standards for radiated emissions.

The UEMR from equipment close to, but not associated with radio telescopes is a day-to-day reality. Like the UEMR from satellites, their spectra are generally tens to hundreds of MHz wide, and have a comb-like structure in addition to a more diffuse wide-band spectrum. This type of UEMR is typically handled in various ways, for example (i) raising awareness with local stakeholders; (ii) advocating for local, regional, and/or national protected geographic radio quiet zones; (iii) establishing bilateral covenants requiring EMC limits stricter than typical levels specified in industry norms such as CISPR-32 and EN 55032 (e.g., wind and solar photovoltaic installations near the LOFAR core[5]); (iv) cooperation with equipment owners to mitigate at the source (mending electric fences, replacing LED lights, switching off CCTV cameras); and/or (v) formal regulatory complaints and follow-up by national administrations in cases of noncooperative parties. The last step is generally only

[5] https://www.rvo.nl/onderwerpen/bureau-energieprojecten/lopende-projecten/windpark-dm-en-om

viable if the sources exceed EMC norms similar to CISPR-32/EN 55032. As far as we are aware, a similar regulatory or normative framework is lacking for space applications. In contrast to satellites, we note that all of these sources are generally greatly attenuated by the telescope as, unlike satellites, they are never directly in its main beam.

In the absence of regulations that address UEMR emission from satellites, the astronomical community will have to raise and address this issue with regulatory bodies as well as satellite operators, and must continue to do so. Fortunately, SpaceX/Starlink is already actively co-operating with both optical astronomy (e.g., Tyson et al. 2020) and radio astronomy (e.g., Nhan et al. 2024) to investigate and/or test mitigation strategies. Our observations and analysis, presenting properties of the UEMR (electric field strengths, emission frequencies, comb properties) of different satellite versions, possibly combined with those of other radio telescopes, may provide information that allows SpaceX/Starlink to identify the satellite components involved in the emission of UEMR and devise mitigation strategies in already operational satellites, as well as future designs of the hardware.

Acknowledgements. We thank Colin Lonsdale for informing us of the presence of UEMR from the second-generation Starlink satellites. We acknowledge fruitful discussions with Jess Dempsey, Michiel van Haarlem and Wim van Cappellen. This paper is based on data obtained with the International LOFAR Telescope (ILT) under project code LC20_009. LOFAR (van Haarlem et al. 2013) is the Low Frequency Array designed and constructed by ASTRON. It has observing, data processing, and data storage facilities in several countries, that are owned by various parties (each with their own funding sources), and that are collectively operated by the ILT foundation under a joint scientific policy. The ILT resources have benefitted from the following recent major funding sources: CNRS-INSU, Observatoire de Paris and Université d'Orléans, France; BMBF, MIWF-NRW, MPG, Germany; Science Foundation Ireland (SFI), Department of Business, Enterprise and Innovation (DBEI), Ireland; NWO, The Netherlands; The Science and Technology Facilities Council, UK; Ministry of Science and Higher Education, Poland. The project leading to this publication has received funding from the European Union's Horizon 2020 research and innovation programme under grant agreement No 101004719. This paper made extensive use of the Python scientific software stack, and we acknowledge the developers of `numpy` (van der Walt et al. 2011), `matplotlib` (Hunter 2007), `scipy` (Jones et al. 2001), `astropy` (Astropy Collaboration 2013, 2022) and `Skyfield` (Rhodes 2019).

References

Astropy Collaboration (Robitaille, T. P., et al.) 2013, A&A, 558, A33
Astropy Collaboration (Price-Whelan, A. M., et al.) 2022, ApJ, 935, 167
Barentine, J. C., Venkatesan, A., Heim, J., et al. 2023, Nat. Astron., 7, 252
Bassa, C. G., Hainaut, O. R., & Galadí-Enríquez, D. 2022, A&A, 657, A75
Bowman, J. D., Rogers, A. E. E., & Hewitt, J. N. 2008, ApJ, 676, 1
Broekema, P. C., Mol, J. J. D., Nijboer, R., et al. 2018, Astron. Comput., 23, 180
CENELEC 2015, EN55032:2015: Electromagnetic Compatibility of Multimedia Equipment - Emission Requirements, Tech. rep. (NEN, Royal Netherlands Standardization Institute)
Di Vruno, F., Winkel, B., Bassa, C. G., et al. 2023, A&A, 676, A75
Green, R. F., Luginbuhl, C. B., Wainscoat, R. J., & Duriscoe, D. 2022, A&ARv, 30, 1
Grigg, D., Tingay, S. J., Sokolowski, M., et al. 2023, A&A, 678, L6
Hainaut, O. R., & Moehler, S. 2024, A&A, 683, A147
Hunter, J. 2007, Comput. Sci. Eng., 9, 90
ITU-R 2003, Protection Criteria used for Radio Astronomical Measurements, Recommendation RA.769-2 (Geneva: International Telecommunication Union)
ITU-R 2007a, Interference Calculations between Non-geostationary Mobile-satellite Service or Radionavigation-satellite Service Systems and Radio Astronomy Telescope Sites, Recommendation M.1583-1 (Geneva: International Telecommunication Union)
ITU-R 2007b, Calculation of Unwanted Emission Levels Produced by a Non-geostationary Fixed-satellite Service System at Radio Astronomy Sites, Recommendation S.1586-1 (Geneva: International Telecommunication Union)
ITU-R 2020, Radio Regulations (Geneva: WRC-19/Sharm el-Sheik)
Jones, E., Oliphant, T., Peterson, P., et al. 2001, SciPy: Open Source Scientific Tools for Python
Kondratiev, V. I., Verbiest, J. P. W., Hessels, J. W. T., et al. 2016, A&A, 585, A128
Kovalev, M., Hainaut, O. R., Chen, X., & Han, Z. 2023, MNRAS, 525, L60
Kruk, S., García-Martín, P., Popescu, M., et al. 2023, Nat. Astron., 7, 262
Lang, T., Spencer, S. T., & Mitchell, A. M. W. 2023, A&A, 677, A141
McDowell, J. C. 2020, ApJ, 892, L36
Michałowski, M. J., Kamiński, K., Kamińska, M. K., & Wnuk, E. 2021, Nat. Astron., 5, 995
Mróz, P., Otarola, A., Prince, T. A., et al. 2022, ApJ, 924, L30
Nhan, B. D., De Pree, C. G., Iverson, M., et al. 2024, ApJ, 971, L49
Offringa, A. R., de Bruyn, A. G., Zaroubi, S., et al. 2013, A&A, 549, A11
Rhodes, B. 2019, Astrophysics Source Code Library [record ascl:1907.024]
Technical committee CISPR/CIS/I Electromagnetic compatibility of information technology equipment, multimedia equipment and receivers 2015, CISPR32:2015: Electromagnetic Compatibility of Multimedia Equipment - Emission Requirements, Tech. rep. (IEC)
Tyson, J. A., Ivezić, Ž., Bradshaw, A., et al. 2020, AJ, 160, 226
van der Walt, S., Colbert, S., & Varoquaux, G. 2011, Comput. Sci. Eng., 13, 22
van Haarlem, M. P., Wise, M. W., Gunst, A. W., et al. 2013, A&A, 556, A2
Walker, C., Di Pippo, S., Aubé, M., et al. 2020a, https://doi.org/10.5281/zenodo.5898785
Walker, C., Hall, J., Allen, L., et al. 2020b, BAAS, 52, 0206
Walker, C., Di Pippo, S., Aubé, M., et al. 2021, https://doi.org/10.5281/zenodo.5874725
Zarka, P., Girard, J. N., Tagger, M., Denis, L., et al. 2012, in SF2A-2012: Proceedings of the Annual meeting of the French Society of Astronomy and Astrophysics, eds. S. Boissier, P. de Laverny, N. Nardetto, et al., 687

Appendix A: Additional figures

This appendix shows figures of aligned and averaged dynamic spectra for Starlink satellites in which UEMR is detected. Figures A.1 and A.2 show detections for Starlink v2-Mini and v2-Mini DTC satellites in the LBA observing band between 10 and 88 MHz. In the HBA band covering 110 to 188 MHz, Figs. A.3 and A.4 show aligned and averaged dynamic spectra for a Starlink v1.5 and a v2-Mini satellite. The color scale of the dynamic spectra is in power flux density.

These dynamic spectra show the UEMR from Starlink satellites, as well as interference from terrestrial sources. Satellite UEMR will stand out because of its temporal signature as the satellite passes through the telescope field-of-view. For comparison, terrestrial RFI is primarily detected through the telescope side-lobes and hence has no specific, nor predictable, variation with time.

Terrestrial RFI in the LOFAR band is primarily due to allocated services, and an overview of these is given in Offringa et al. (2013). In the LBA band from 10 to 88 MHz, these services predominantly affect frequencies below 30 MHz, where beyond the horizon transmissions are detectable through reflections off the ionosphere. In the HBA band from 110 to 188 MHz, digital audio broadcasting channels continuously occupy frequencies in several 1.6 MHz wide bands from 174 MHz and higher, while air traffic control (118 to 137 MHz), satellite downlinks (137 to 138 MHz) and amateur radio (144 to 146 MHz) use smaller bandwidths (a few kHz) and transmit for limited time periods (seconds to minutes).

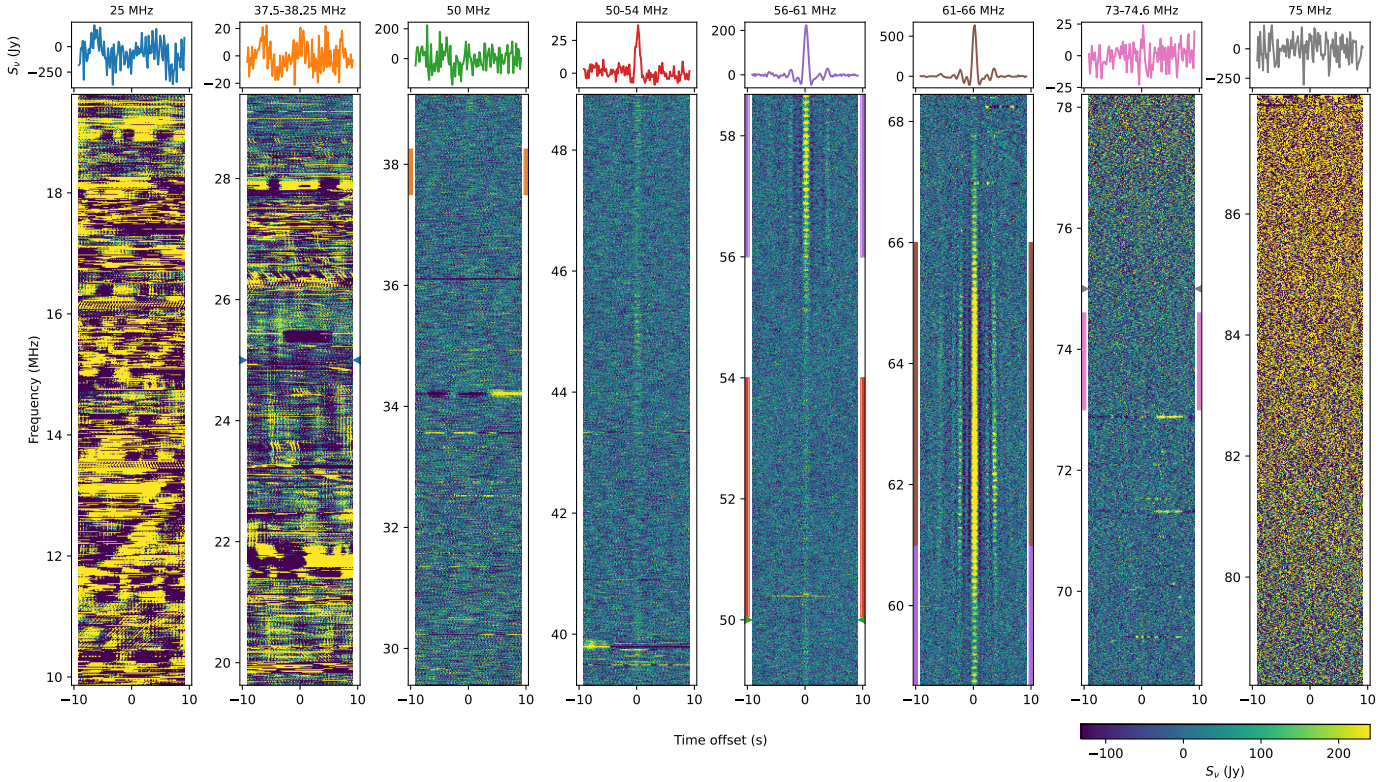

Fig. A.1. Spectral and temporal properties of the passage of the Starlink v2-Mini satellite Starlink-31441 [60091/2024-117A] (average of 11 TABs) in the LBA band from 10 to 88 MHz. Normalized, aligned, and averaged dynamic spectra (in power flux density units) are shown over the entire observed bandwidth and are centered on the predicted passage time of the satellite. Time series at specific narrowband frequencies and broadband frequency ranges are shown in the top insets. The color of each time series matches the marked frequencies and frequency ranges, in the same colors as the sides of the dynamic spectra.

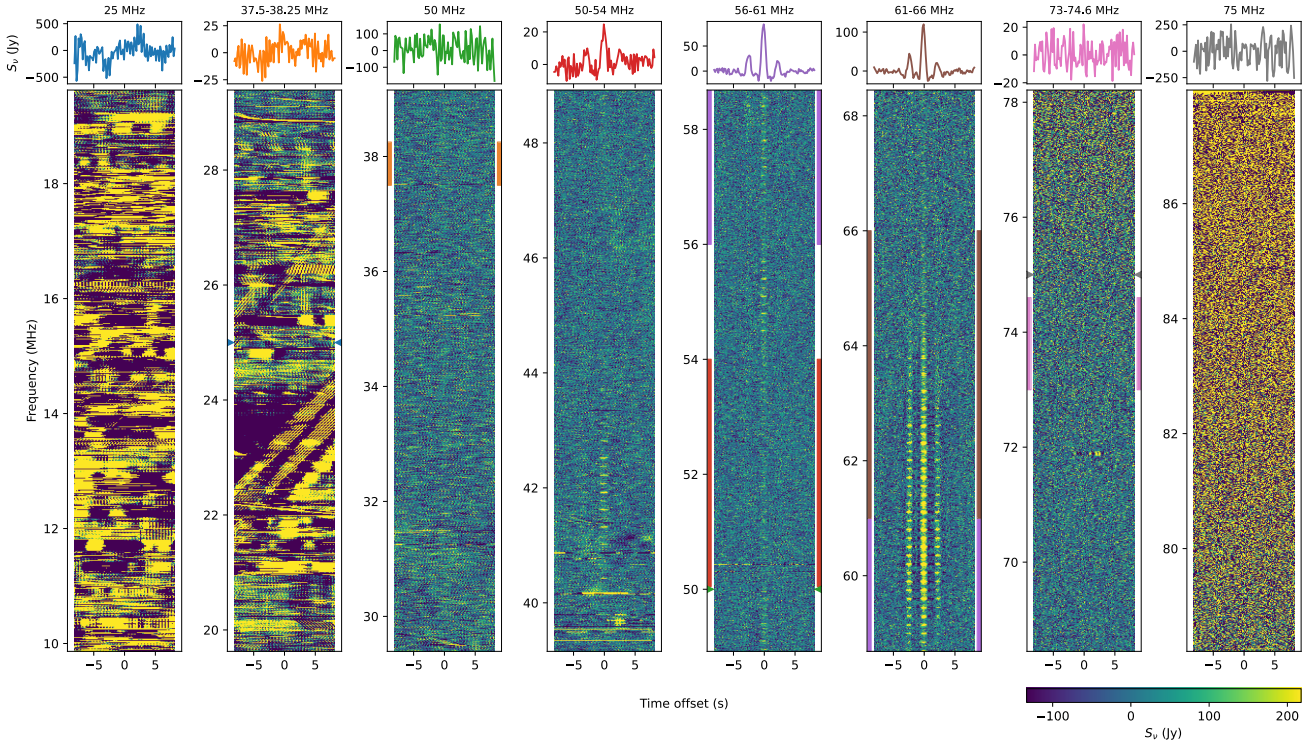

Fig. A.2. Spectral and temporal properties of the passage of the Starlink v2-Mini DTC satellite Starlink-11133 [DTC] [59954/2024-107K] (average of 11 TABs) in the LBA band from 10 to 88 MHz.

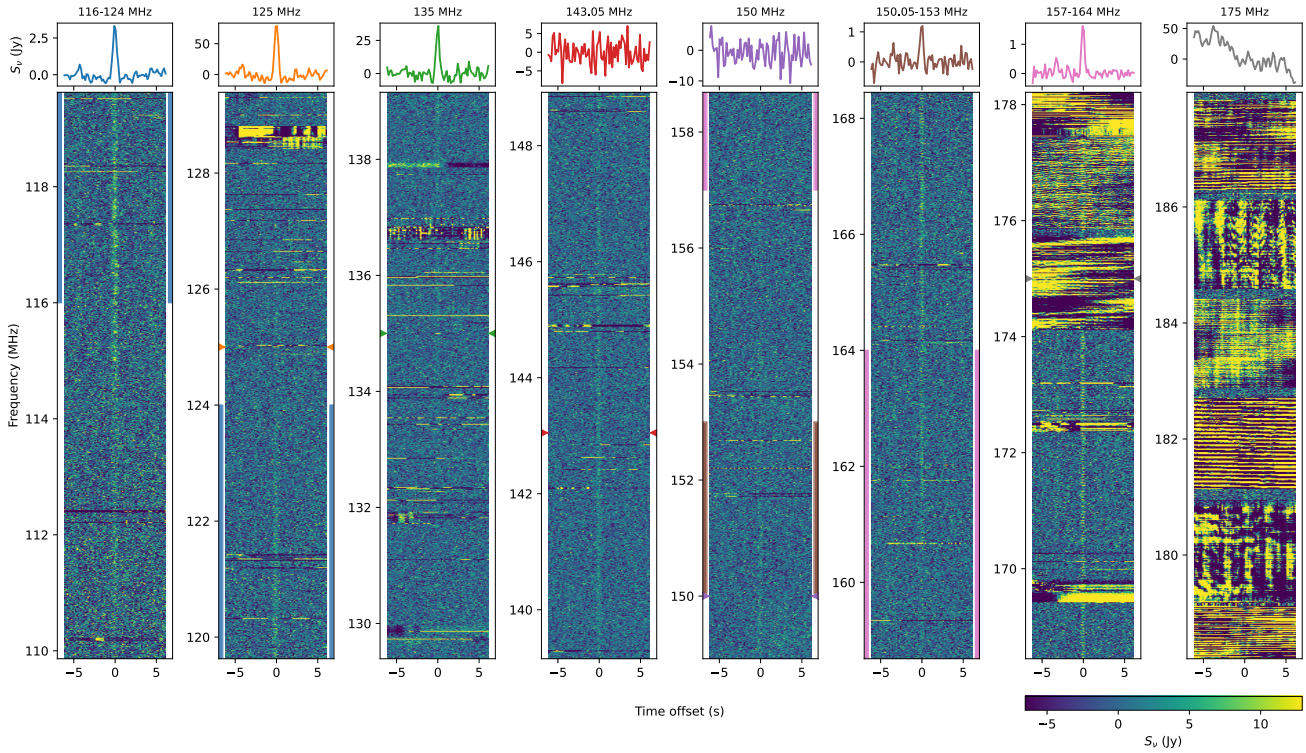

Fig. A.3. Spectral and temporal properties of the passage of of Starlink v1.5 satellite Starlink-3349 [50813/2022-001L] (average of 11 TABs) in the HBA band from 110 to 188 MHz.

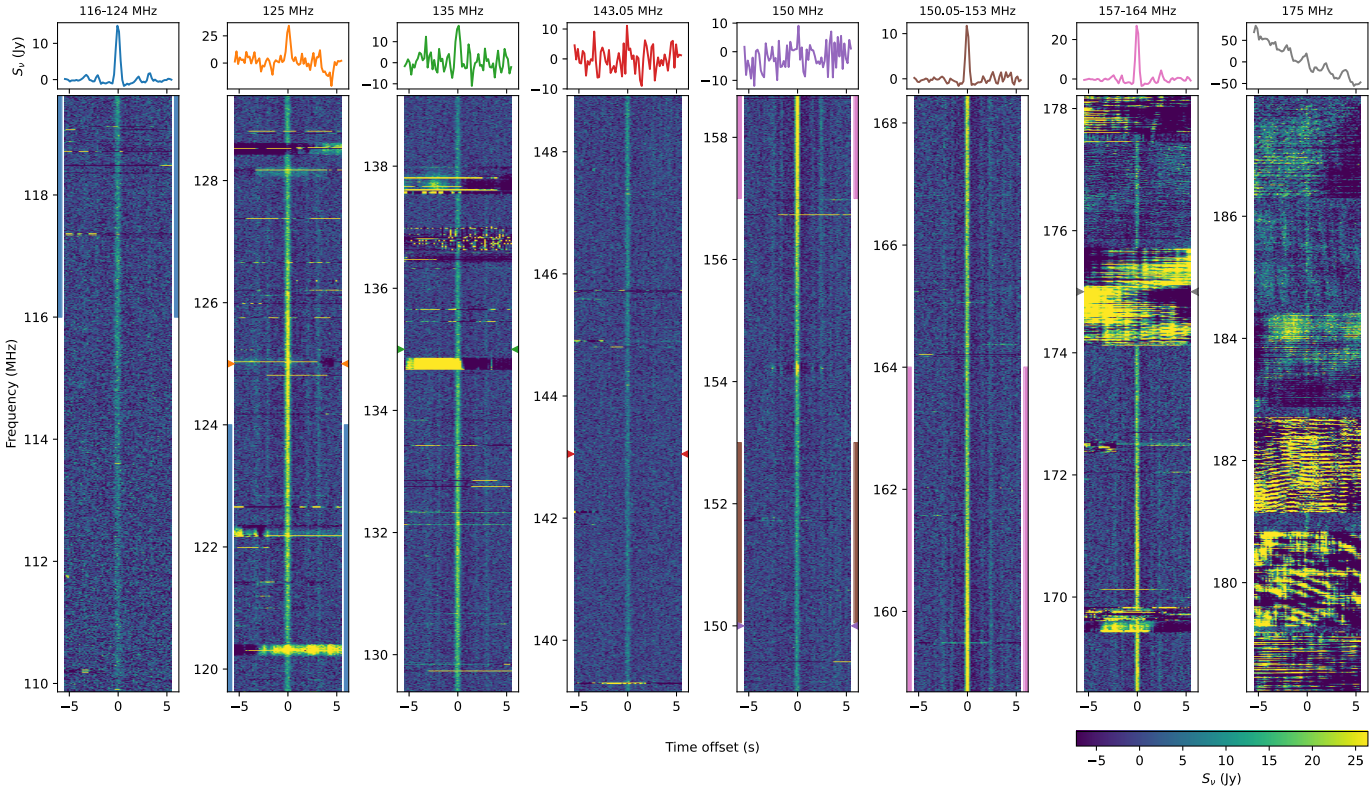

Fig. A.4. Spectral and temporal properties of the passage of of Starlink v2-Mini satellite Starlink-30518 [58029/2023-156B] (average of 11 TABs) in the HBA band from 110 to 188 MHz.

Appendix B: Tables

Table B.1. Second-generation Starlink satellites that have been detected between 10 and 88 MHz.

NORAD / COSPAR	Name	d (km)	$t_{\rm mid}$ (s)	$n_{\rm TAB}$	S_ν (Jy) 50–54 (MHz)	56–61 (MHz)	61–66 (MHz)
57946/2023-148M	STARLINK-30704	558.0	740.14	11		57.9	26.8
58532/2023-192B	STARLINK-31035	490.1	3322.12	11	25.5	235.8	25.1
58543/2023-192N	STARLINK-31049	489.4	3291.96	11	24.6	142.0	61.7
58544/2023-192P	STARLINK-31048	488.9	2902.19	11	39.4	361.8	67.6
58545/2023-192Q	STARLINK-31057	488.3	2875.42	11	41.1	413.0	45.1
58546/2023-192R	STARLINK-31050	487.8	2455.88	10	20.9	140.9	50.0
58548/2023-192T	STARLINK-31016	487.6	2063.28	10	14.4	102.7	16.4
58549/2023-192U	STARLINK-31053	487.4	2036.87	2			
58551/2023-192W	STARLINK-30999	489.3	1954.86	8	15.9	73.0	27.8
59949/2024-107E	STARLINK-11138 [DTC]	345.9	2762.60	11	70.3	209.1	160.4
59950/2024-107F	STARLINK-11130 [DTC]	349.5	3290.90	10	27.1	52.7	63.5
59951/2024-107G	STARLINK-11126 [DTC]	347.2	3110.70	11	23.5	64.7	106.2
59952/2024-107H	STARLINK-11124 [DTC]	347.9	2928.68	11	39.5	99.7	153.5
59953/2024-107J	STARLINK-11143 [DTC]	346.8	2749.49	11	53.1	115.0	160.7
59954/2024-107K	STARLINK-11133 [DTC]	345.9	2569.45	11	26.5	107.9	128.5
59955/2024-107L	STARLINK-11144 [DTC]	345.6	2389.55	10	15.0	23.8	26.2
59956/2024-107M	STARLINK-11134 [DTC]	345.0	2209.46	2			
60091/2024-117A	STARLINK-31441	388.2	353.10	11	40.0	255.8	686.8
60092/2024-117B	STARLINK-32044	388.5	322.46	11	50.2	319.8	445.8
60093/2024-117C	STARLINK-31239	387.6	279.19	11	59.4	221.7	996.7
60094/2024-117D	STARLINK-32007	388.7	261.57	11	151.5	1273.6	990.3
60095/2024-117E	STARLINK-32028	388.5	231.09	11	65.2	255.5	620.5
60096/2024-117F	STARLINK-32016	388.6	200.64	11	65.9	354.8	887.4
60097/2024-117G	STARLINK-32003	388.9	170.23	11	50.7	189.2	458.5
60098/2024-117H	STARLINK-32026	389.0	109.19	11	67.9	210.9	941.7
60099/2024-117J	STARLINK-31732	388.9	139.72	11	75.5	447.3	1074.8
60100/2024-117K	STARLINK-31996	389.3	78.75	11	77.3	235.1	399.1
60101/2024-117L	STARLINK-31999	389.2	48.16	11	62.5	375.3	680.8
60102/2024-117M	STARLINK-31954	389.6	12.58	11	81.8	242.4	486.1

Notes. Satellites are identified by their NORAD catalog numer and the COSPAR international designator, which provides the launch year, launch number, and sequential identifier, and by their name. Satellites with [DTC] in their name are of the v2-Mini direct-to-cell (DTC) version; all other satellites are of the v2-Mini version. For each satellite the distance (d in km), passage mid-point ($t_{\rm mid}$ in s) during the 1 hr observation (which started on July 19, 2024, at 06:00 UTC) and the number of tied-array beams the satellite passed through ($n_{\rm TAB}$) are provided. Power flux density measurements (S_ν in Jy) are given for three frequency ranges.

Table B.2. First-generation Starlink satellites that have been detected between 110 and 188 MHz.

NORAD / COSPAR	Name	d (km)	$t_{\rm mid}$ (s)	$n_{\rm TAB}$	S_ν (Jy) 116–124 (MHz)	125 (MHz)	135 (MHz)	150 (MHz)	150.05–153 (MHz)	157–165 (MHz)
Starlink v1.0										
45103/2020-006BM	STARLINK-1196	383.4	539.83	11	0.7					0.9
45362/2020-019C	STARLINK-1306	553.2	2469.55	11	2.9	167.3	34.7	14.9	0.9	
45366/2020-019G	STARLINK-1262	553.9	1146.02	11	3.0	200.7	30.8	10.1	2.9	2.3
45367/2020-019H	STARLINK-1273	553.8	3131.25	2	2.9				1.3	
45368/2020-019J	STARLINK-1276	554.2	485.78	11	3.3	244.4	48.7	22.1	1.0	0.6
45373/2020-019P	STARLINK-1295	553.6	1808.10	11	2.9	191.6	17.0	12.8	0.5	0.4
45374/2020-019Q	STARLINK-1300	553.7	1477.32	11	3.2	178.4	31.6	20.0	1.3	0.7
45375/2020-019R	STARLINK-1302	553.5	2800.60	11	2.5	153.9	25.2	10.5	0.8	
45377/2020-019T	STARLINK-1305	554.0	815.43	11	2.9	192.2	18.9	23.8	1.2	0.8
45379/2020-019V	STARLINK-1319	554.5	155.49	11	2.7	139.2			0.9	0.4
45770/2020-038AS	STARLINK-1462	419.9	3104.90	11					1.3	0.7
46542/2020-070L	STARLINK-1692	554.2	3280.05	12	3.1	159.1	35.9	12.3	2.0	0.6
46544/2020-070N	STARLINK-1694	552.8	1733.87	6	2.5	79.2			0.7	
46550/2020-070U	STARLINK-1701	554.0	2950.69	11	2.7	192.3	23.0		1.1	
46554/2020-070Y	STARLINK-1671	554.1	743.25	11	0.6				0.7	
46561/2020-070AF	STARLINK-1709	552.9	1648.75	9	2.8	134.4	21.7		1.2	
46563/2020-070AH	STARLINK-1730	554.5	4.94	11	3.1	187.0	24.6		1.1	0.3
46572/2020-070AS	STARLINK-1531	552.9	2204.51	6	2.9	131.1	24.2			
46577/2020-070AX	STARLINK-1682	553.3	1071.23	11	3.3	178.7	23.1			
46586/2020-070BG	STARLINK-1737	553.8	335.48	9	2.4	91.9				
48093/2021-027B	STARLINK-2404	554.5	410.49	11	4.5	150.2	21.2		1.5	
48094/2021-027C	STARLINK-2412	553.4	1883.94	11	4.6	149.2	86.2		1.4	0.8
48095/2021-027D	STARLINK-2414	553.9	2543.80	11	4.7	135.1	40.6		1.9	
48099/2021-027H	STARLINK-2428	553.2	1222.05	11	4.2	125.0	29.7		1.1	
48111/2021-027V	STARLINK-2448	553.2	1402.33	11	4.0	146.0	22.2		1.4	0.3
48113/2021-027X	STARLINK-2450	553.3	891.38	3	2.3	107.7	32.5			
48115/2021-027Z	STARLINK-2452	555.0	79.21	11	3.5	158.9	26.2		1.2	0.5
48130/2021-027AQ	STARLINK-2472	553.4	2620.26	10	2.8	163.7	21.4	13.9	1.0	0.6
48133/2021-027AT	STARLINK-2475	554.7	3536.29	11	4.3	158.2		13.3	1.0	0.3
48134/2021-027AU	STARLINK-2476	553.7	2213.20	11	3.2	148.7	28.5		0.8	
48135/2021-027AV	STARLINK-2478	552.9	2288.87	6	3.5	321.6	33.3		2.9	
48136/2021-027AW	STARLINK-2479	554.3	2875.03	11	2.9	89.8	16.8			
48138/2021-027AY	STARLINK-2481	554.6	3205.66	11	2.9	154.1	18.6	14.0	1.0	0.3
48141/2021-027BB	STARLINK-2484	553.3	1552.86	11	4.5	145.2	28.8		2.0	
48435/2021-040H	STARLINK-2633	553.4	2139.10	11	4.3	150.6	22.5		1.9	
Starlink v1.5										
49730/2021-115G	STARLINK-3249	545.5	1874.18	3	3.6	102.2				
49733/2021-115K	STARLINK-3252	548.2	553.31	7	2.2	100.2	38.3			0.8
49739/2021-115R	STARLINK-3155	545.8	1543.50	11	2.4	67.4	34.1		0.8	1.8
50803/2022-001A	STARLINK-3321	547.6	1032.03	3	1.6	83.6	34.5			
50813/2022-001L	STARLINK-3349	546.4	1213.78	11	3.5	83.6	30.9		1.0	1.4
50815/2022-001N	STARLINK-3234	547.4	701.90	9	2.3	83.5	51.5		0.6	
50817/2022-001Q	STARLINK-3341	547.3	371.80	11	3.0	43.4	33.7		1.0	1.8
50822/2022-001V	STARLINK-3343	548.0	3014.22	4	2.4	80.0	30.4			
50823/2022-001W	STARLINK-3334	547.3	40.97	11	2.0	86.1	48.2		0.8	0.4
50825/2022-001Y	STARLINK-3332	547.9	3344.32	11	3.1	84.5	55.2			1.4
50828/2022-001AB	STARLINK-3290	547.9	3099.60	7	2.2	94.8	51.6			
50836/2022-001AK	STARLINK-3330	548.8	3578.54	4	2.1		45.8			
50839/2022-001AN	STARLINK-3320	548.6	3492.75	6	2.2	73.8	51.5			
50840/2022-001AP	STARLINK-3295	547.6	3162.72	10	2.1	102.3	37.8	6.8	1.0	
50842/2022-001AR	STARLINK-3302	546.7	2832.29	11	3.4	109.4	84.8			
50846/2022-001AV	STARLINK-3308	546.1	2502.19	12	2.6	70.9	58.6		0.5	
50849/2022-001AY	STARLINK-3311	545.5	2171.94	4	2.6		35.6			
52669/2022-053P	STARLINK-3972	546.4	477.68	5	1.5	101.5	30.8		0.8	
52671/2022-053R	STARLINK-4071	547.2	148.46	11	1.5	104.7	34.3	12.1	0.5	1.0
53132/2022-083A	STARLINK-4063	547.2	2097.51	6	2.7	114.6	39.7	16.1	0.9	0.8
53137/2022-083F	STARLINK-4145	547.7	2427.57	1	1.7	66.2				
53139/2022-083H	STARLINK-4185	546.3	1436.86	11	2.1	122.2	28.1	24.1		1.0
53140/2022-083J	STARLINK-4170	546.7	1767.16	11	2.8	92.7	70.2	13.0		0.8
53142/2022-083L	STARLINK-4101	546.0	861.97	1	2.5	75.3				
53151/2022-083V	STARLINK-4040	546.6	2278.75	11	1.2	98.7	85.0		0.8	
53152/2022-083W	STARLINK-4045	546.4	2939.61	8	1.9	106.9	28.1			0.5
53153/2022-083X	STARLINK-4098	547.0	1948.56	7	2.3	96.1				
53154/2022-083Y	STARLINK-4077	546.4	2609.52	11	1.7	155.0	36.1	11.3	1.4	0.7
53158/2022-083AC	STARLINK-4054	547.4	1617.95	1	1.9					1.4
53170/2022-083AQ	STARLINK-4095	547.0	883.27	11	1.5	114.8	30.4			
53172/2022-083AS	STARLINK-4299	548.7	223.01	1	2.6	97.0				
53684/2022-105AN	STARLINK-4624	571.0	3551.23	2	1.8	75.4	33.2			

Notes. Satellite versions v1.0 and v1.5 are as indicated. The column descriptions are otherwise identical to those in Table B.1.

Table B.3. Second-generation Starlink satellites that have been detected between 110 and 188 MHz.

NORAD / COSPAR	Name	d (km)	$t_{\rm mid}$ (s)	$n_{\rm TAB}$	S_ν (Jy) 116–124 (MHz)	150.05–153 (MHz)	157–165 (MHz)
58028/2023-156A	STARLINK-30514	489.3	3233.81	11	12.6	10.8	10.4
58029/2023-156B	STARLINK-30518	488.2	2814.52	11	16.0	9.6	20.2
58030/2023-156C	STARLINK-30549	489.1	2779.45	10	10.6	12.4	24.8
58531/2023-192A	STARLINK-31012	488.0	845.05	12	3.6	59.4	76.9
58535/2023-192E	STARLINK-31032	489.2	425.75	11	6.2	60.7	93.4
58541/2023-192L	STARLINK-31045	558.7	1663.61	10	3.2	23.8	39.7
59000/2024-036C	STARLINK-31529	490.2	3575.53	5	3.5	37.9	34.4
59003/2024-036F	STARLINK-31429	489.4	1898.36	1	3.6	49.3	43.0
59009/2024-036M	STARLINK-31488	489.1	1868.27	1	1.8	52.3	60.1
59010/2024-036N	STARLINK-31528	481.4	1331.45	11	6.7	37.1	57.1
59011/2024-036P	STARLINK-31491	482.3	1425.33	10	6.6	41.3	60.7
59012/2024-036Q	STARLINK-31465	482.4	951.62	12	4.8	40.6	80.7
59013/2024-036R	STARLINK-31389	488.1	1029.53	11	5.0	62.6	64.9
59014/2024-036S	STARLINK-31454	486.9	639.58	11	105.6	37.5	96.0
59015/2024-036T	STARLINK-31521	481.9	572.74	8	9.1	4.0	4.6
59016/2024-036U	STARLINK-31526	453.2	1143.53	8	6.1	39.0	69.7
59962/2024-107T	STARLINK-31980	454.3	1572.30	6	10.5	45.7	72.8
59964/2024-107V	STARLINK-31979	453.7	2018.05	11	7.6	50.8	76.9
60017/2024-111B	STARLINK-31987	454.4	2134.08	6	5.8	50.7	80.8
60024/2024-111J	STARLINK-31990	453.8	1747.35	11	6.5	59.5	93.8
60029/2024-111P	STARLINK-32006	454.5	2163.51	4	5.0	51.7	70.8
60032/2024-111S	STARLINK-32017	453.2	1301.68	11	8.8	17.1	20.7
60033/2024-111T	STARLINK-31998	453.7	1717.76	11	5.0	49.6	93.8
60039/2024-112B	STARLINK-11140 [DTC]	348.3	1203.93	3	20.2	10.3	7.8
60040/2024-112C	STARLINK-11122 [DTC]	346.9	1010.02	10	40.0	14.8	9.5
60041/2024-112D	STARLINK-11149 [DTC]	346.6	827.23	11	42.5	19.5	11.2
60042/2024-112E	STARLINK-11120 [DTC]	345.4	635.82	11	15.7	84.9	
60043/2024-112F	STARLINK-11086 [DTC]	347.0	451.20	6	29.2	5.3	3.2
60048/2024-112L	STARLINK-11135 [DTC]	348.5	943.22	5	81.4	8.3	7.3
60054/2024-112S	STARLINK-31735	454.3	2584.05	7	10.5	43.5	71.5

Notes. Satellites with [DTC] in their name are of the v2-Mini direct-to-cell (DTC) version, all other satellites are of the v2-Mini version. The column descriptions are otherwise identical to those of Table B.1. The passage mid-point times $t_{\rm mid}$ are with respect to the observation start time of July 19, 2024, at 07:30 UTC.